Chapter 6

Fatty Acid and Phospholipid Crystalline Adsorbates: Ultrafast T-jump Dynamics*

To study the dynamics of the surface adsorbates of crystalline fatty acids and phospholipids, the diffraction patterns were followed as a function of time after ultrafast laser irradiation. Earlier femtosecond spectroscopie studies have provided valuable information about the dynamics on the picosecond timescale, but could not determine the structure [134, 135]. Time-resolved X-ray diffraction studies showed a laser-induced ultrafast melting in fatty acid films above the damage threshold [136]. However, the results were not for monolayers and bilayers, and for the sample used (83 layers), a drawback is the inevitable destruction of the films. To our knowledge, the only reported nondestructive technique used to resolve the structure and dynamics is UEC.

In our experiments, the fatty acids and phospholipids have no absorption resonance at the excitation wavelength of 800nm and thus appear transparent, with the energy being absorbed solely by the silicon substrate. The mechanism of heating the substrate is discussed in chapter 4. Following the initial formation of electron hole pairs, the energy is transferred in a few picoseconds to the lattice through electron-phonon coupling, thereby virtually creating a temperature jump in the silicon substrate. Through coupling of the substrate to the fatty acid or phospholipid molecules the energy is also transferred into the adsorbate, where unique structural changes are

*This chapter is based on the work presented in references [28, 29, 71].

induced at far-from-equilibrium temperatures.

At negative time delays, i.e., when the electrons arrive before the laser pulses, the observed diffraction frames are the same as those obtained at steady-state, i.e., the static diffraction patterns. The frames at negative times serve as reference for the subsequent changes with time. At positive time delays, we probe the structural changes of the adsorbate as a result of the temperature jump in the underlying substrate. For every time frame, each Bragg spot was fitted with a Voigt line shape function in the vertical and horizontal direction, respectively, after careful removal of the background, which results mainly from incoherent, inelastic and other scattering. This fitting procedure provides with precision the center position and the width as a function of time. The determination of the center position proved to be insensitive to background subtraction, because of the large intensity of diffraction spots relative to the background; for the line width accurate background removal and good signal-to-noise ratio determine the accuracy of the values obtained. The intensities of Bragg spots were obtained by gating with a window of pixels on the CCD and integrate it to give the changes with time; the gate remains the same for all frames.

6.1 Fatty acids structural dynamics

Figure 6.1 shows a typical time dependent diffraction difference frames of the (002) Bragg spot, with respect to the diffraction image before time zero, recorded for the bilayer film deposited at pH = 9 and $\pi = 10$ mN/m at low incidence angle ($\theta_i = 0.8°$, $\phi = 0°$). As expected, the diffraction difference frame at negative time delay (-20 ps) does not show any features, i.e., there is no change before time zero. Immediately after the heating pulse (0 ps and 1 ps), an intensity loss of the Bragg spots is observed, as dark spots appear in the difference frames. The change in the Bragg spots becomes more prominent over time (10–100 ps). The lower part of the peaks becomes brighter while the upper part becomes darker, showing a downward shift of the Bragg spots. With extended time delays (200–1110 ps), the difference patterns get fainter again, indicating that the peaks are moving back to their original position. This be-

havior confirms that both the heating and electron pulses, because of their ultrashort durations and fluxes, do not damage the bilayer. It should be emphasized, that the structural change is observed only in the direction perpendicular to the shadow edge of the diffraction pattern, i.e., in the vertical direction of the momentum transfer s-coordinate. A similar behavior is observed for all diffraction of all the fatty acid films studied, regardless of ϕ and θ_i.

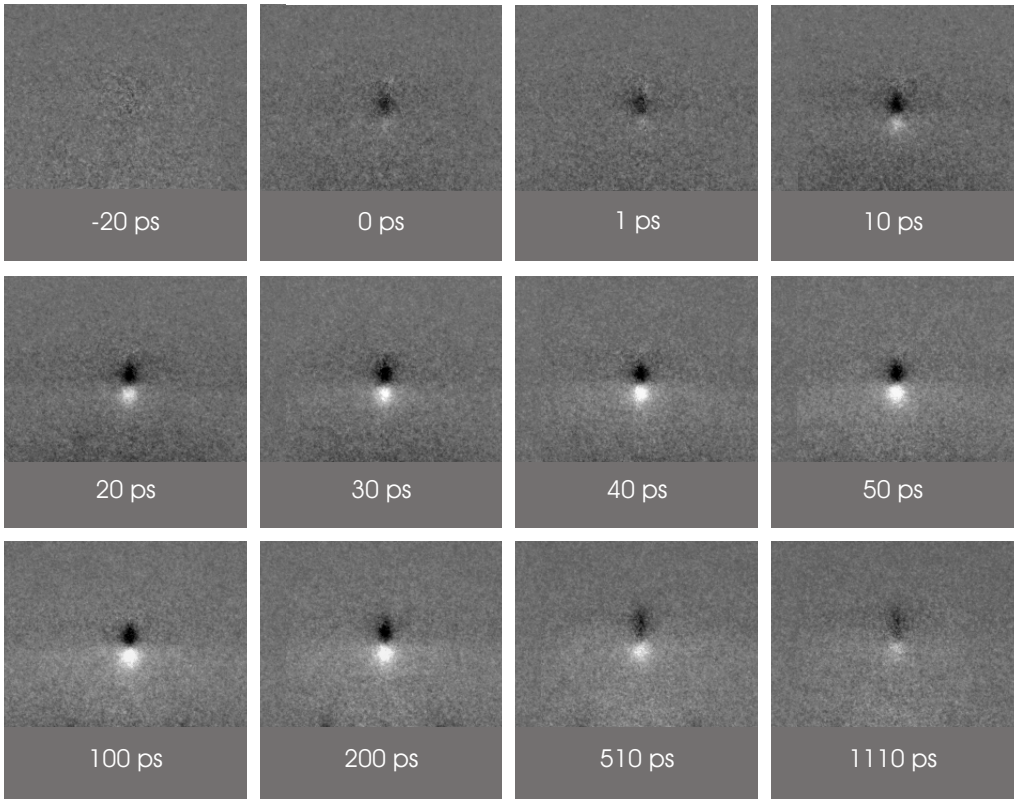

Figure 6.1: Diffraction difference frames of the (002) Bragg spot at various time delays for the bilayer film deposited at pH = 9 and $\pi = 10$ mN/m, obtained at low incidence angle ($\theta_i = 0.8°$, $\phi = 0°$) [28, 71].

In figure 6.2, we show examples of the detailed analysis of the (002) Bragg spot, here for the 4-layer sample deposited at pH = 6.4 and $\pi = 29$ mN/m. As depicted in figure 6.2 (A), for a delay time as long as $t = 1000$ ps the fit of the Bragg spot with a Voigt line shape function in the vertical direction is very good; the same is true for all other time delays. From such excellent data sets the exact center position change, the

relative integrated intensity and full width at half maximum (FWHM) were obtained as a function of time (shown in figure 6.2(B), (C) and (D), respectively). We observed similar trends for all Bragg spots in each sample under investigation. We note that each Bragg spot was found to fit well to a Voigt line shape function in the horizontal or vertical direction after careful removal of the background. However, for the data sets with less than optimal quality samples, the line width changes with time were sometimes obscured by the noise.

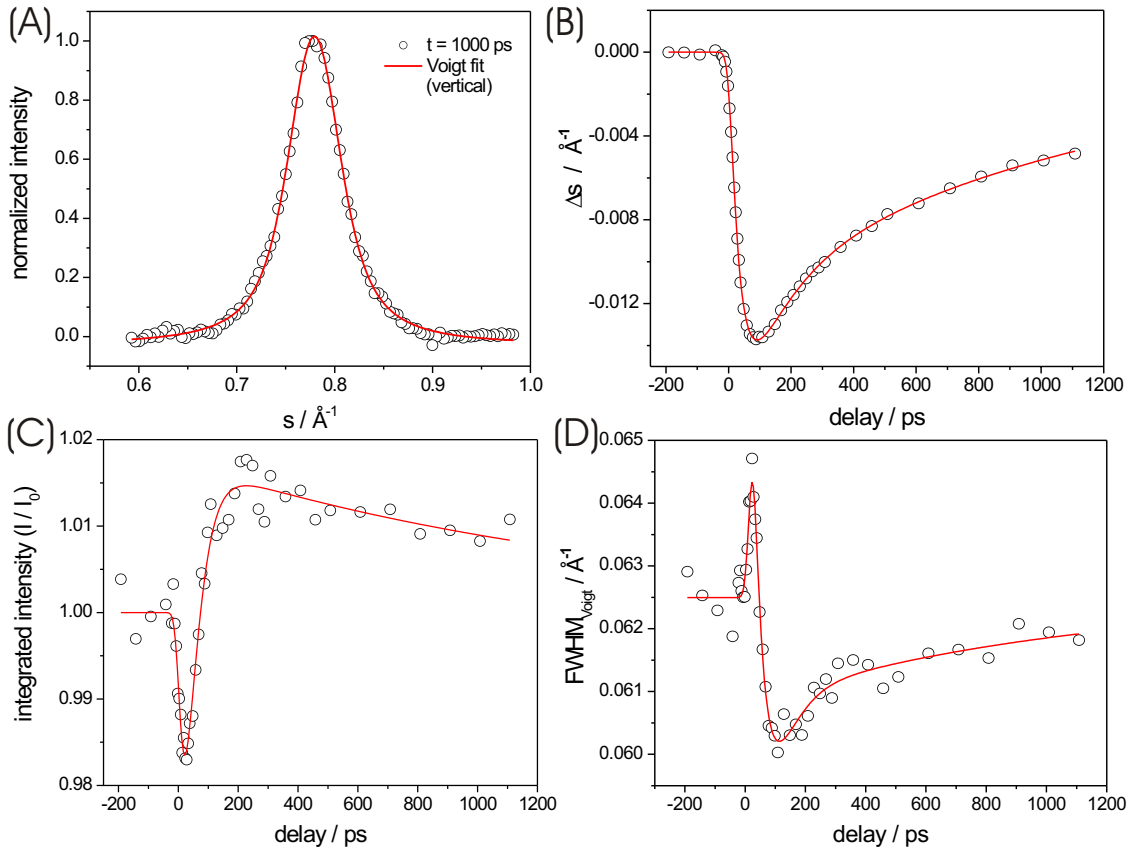

Figure 6.2: Full analysis of the (002) Bragg spot of the 4-layer calcium arachidate sample deposited at pH = 6.4 and $\pi = 29$ mN/m for $\phi = 90°$ and $\theta_i = 0.4°$. (A) Representative Voigt fit of the normalized (002) Bragg spot in the vertical direction at $t = 1000$ ps, after background removal. (B) The momentum transfer change Δs in the vertical direction as a function of time. (C) Relative intensity change I/I_0 as a function of time. (D) Full width at half maximum (FWHM) for the (002) Bragg spot as a function of time [71].

The most pronounced dynamical features of the diffraction patterns after the ultrafast temperature jump are the collective downward movement of the Bragg spots

and subsequent recovery at longer times (figure 6.2(B)); the unusual intensity changes (figure 6.2(C)); and width changes (figure 6.2(D)), which are almost mirror images to the intensity changes, as a function of time.

6.1.1 Atomic motions in the chain

A downshift of Bragg spots in reciprocal space corresponds to an expansion of the orthorhombic R(001) subunit cell along c_0 in real space. There is no measurable change in any of the in-plane directions, that is along a_0 and b_0. This is in contrast to the observations made in the steady-state temperature dependence studies (see section 5.4), and indicates a nonthermal behavior of the LB films on the ultrafast timescale.

A typical time dependent peak shift of the Bragg spots in the vertical direction compared to their original position is depicted in figure 6.3(A) as the z-component of the momentum transfer s versus delay time. It is obtained for the bilayer film deposited at pH = 9 and $\pi = 10$ mN/m at low incidence angle ($\theta_i = 0.8°$, $\phi = 0°$), as the static diffraction pattern shown in figure 5.4(A). As is readily seen, the five Bragg spots all move down and then come back with similar time dependencies. However, there is a relatively small difference between the spots with Miller indices $l = 1$ (e.g., $(0\bar{2}1)$ and (021)) and $l = 2$ (e.g., $(0\bar{2}2)$, (002) and (022)).

As we converted the peak shift into real space, the resulting change in lattice spacing Δc_0, which is the change of -CH_2-CH_2-CH_2- distances of chains, is plotted against time in figure 6.3(B). The plot shows an ultrafast rise of Δc_0, followed by a slower decay. This behavior represents an initial expansion of the sub-cell in the bilayer after impulsive laser-pulse heating of the substrate followed by a subsequent compression due to the heat dissipation. The absolute change Δc_0 is 0.10 and 0.05 Å in the diffraction orders with $l = 1$ and $l = 2$, respectively. For $l = 1$, the change is 4% of the static value $c_0 = 2.54$ Å. For the same l, the expansion of the bilayer takes place with a time constant of 25 ps, whereas the subsequent compression occurs with 55 ps. For the other spots the behavior is similar, and for all peaks, the much longer time behavior is well described with a restructuring time constant of 1.15 ns.

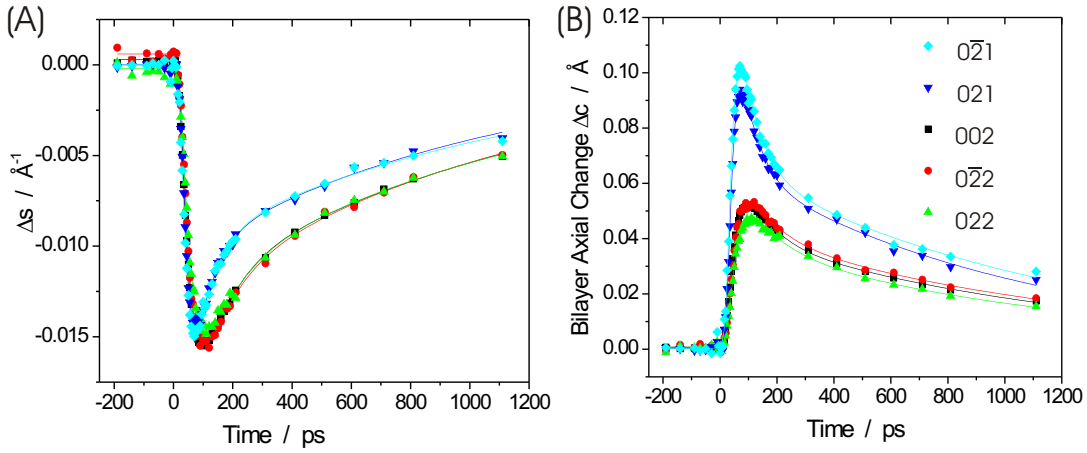

Figure 6.3: Time dependence of the peak shift and the corresponding molecular axial length change, obtained for the bilayer film deposited at pH = 9 and $\pi = 10$ mN/m at low incidence angle ($\theta_i = 0.8°$, $\phi = 0°$). (A) The z-component change Δs of the momentum transfer as a function of time for the different Bragg spots indexed in the diffraction patterns. (B) The corresponding molecular axial length change Δc_0 of the CH_2 sub-cell as a function of time [28].

It seemed obvious to propose that the fact that the Bragg spots of different order $l = 1$ and $l = 2$ move down for almost same amount in s is due to an electric field effect. However, close inspection makes this explanation not likely. First of all, the fatty acid LB films are insulators. The 800nm ultrafast laser did not excite the molecules directly, nor did the influence used in our experiments large enough to break the dielectrics. It seems unlikely that there are free carriers present at the film surfaces. Secondly, the diffraction patterns are generated from the electrons transmitted through the LB films. The simple estimation, assuming the peak shift is due to the electric field from a dipole layer, yields a field strength for 10^7 V/cm and 5×10^{12} electrons at the film surfaces, which seems too large to be possible. Finally, we note that even for the substrate, the rocking curve provides the correct lattice spacing only from higher order diffraction spots (large θ_i's), which have small widths, and therefore care has to be taken at small θ_i's when considering changes in s and the associated larger uncertainty (see section 4.1). We also observed that the downshift of the Si Bragg spots is different from the LB films' (see below), which indicates that

the shift is not due to an electric field effect.

It is interesting to compare the structural dynamics, e.g., the Bragg spots' position changes, in the fatty acid films with that in the silicon substrate. As shown in figure 6.4(A), the diffraction pattern for the bilayer film deposited at pH = 9 and π = 10 mN/m, obtained at $\theta_i = 2.3°$ and $\phi = 1°$ off the Si[11$\bar{2}$] zone axis, was followed as a function of time. At this higher θ_i angle, Bragg spots from the bilayer ((002) Bragg spot) as well as the silicon substrate can be observed, making the comparison straightforward. In the diffraction pattern, the Bragg spots of silicon are indexed in terms of the (111) surface in the zone axis of [11$\bar{2}$]. At this angle Si(00) can also be indexed in terms of the bulk structure as Si(444), as from the rocking curve (figure 5.5).

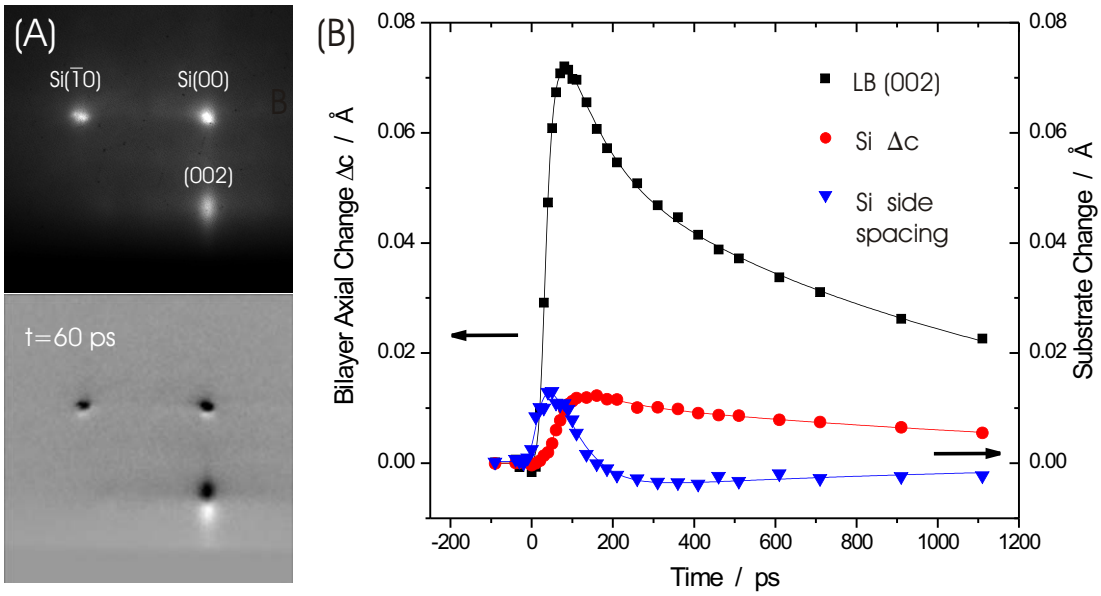

Figure 6.4: Dynamics of fatty acid bilayer compared to that of the substrate Si(111) surface. (A) The static diffraction pattern and the diffraction difference at delay time $t = 60$ ps, obtained at $\theta_i = 2.3°$ and $\phi = 1°$. The s-range is from -0.85 to +0.35 Å^{-1} in horizontal and from +0.45 to +1.65 Å^{-1} in vertical direction. (B) The change of the CH_2 sub-cell in the bilayer and of the substrate. The LB bilayer Δc_0 is obtained from momentum transfer s-values of the Bragg spots (002); the Si Δc from s of the Bragg spots Si(00); and Si side spacing from s of the Bragg spots Si($\bar{1}$0) and Si(00) [28].

The Bragg spots were analyzed in a similar way as for the lower θ_i angles. The

change of the lattice constant in the bilayer and silicon as a function of time are shown in figure 6.4(B). As expected, the LB(002) peak shows the same behavior as in figure 6.3(B). However the silicon lattice undergoes a very different dynamics. While the spot LB(002) of the bilayer changes only in the vertical direction, the spots of the silicon change also sideways, indicating a displacement in the planes parallel to the interface. The absolute change in the lattice spacing is much smaller in silicon than in the bilayer, 0.013 Å (from the (002) spot) vs. 0.072 Å. The temporal behavior indicates the temperature rise, similar to the behavior observed before (see chapter 4); following the rise, the silicon restructures on the nanosecond time scale. The presence of the bilayer on the surface enhances the vibrational couplings (faster rise) and suppresses the large amplitude surface displacement of silicon without the bilayer.

The effect of multilayers on the expansion is shown in figure 6.5 for each Bragg spot in the diffraction pattern at $\phi = 90°$ for the 2-, 4- and 8-layer samples. The data for $\phi = 0°$ are not shown, but the dynamical behavior is similar. The amplitude increases with overall chain length, which is not expected for the dynamics in simple equilibrium. However, as will be discussed in section 6.3, it is consistent with dynamics in the nonequilibrium regime. We must also take into account that LB films show an increased density of "defects" and holes upon increasing thickness (mainly in the outer layers) [88]. As mentioned in chapter 5, in static LB film structures, the decreased influence of substrate has the consequence of in-plane expansion of the subunit cell along a_0 and b_0, the onset of chain inclination, and the loss of crystalline order. The decreased density in LB films upon going from single to multiple layers results in a less confined environment, with the expansion along the carbon chains becoming freer. Spatial confinement indeed decreases the mobility of say a chromophore in the membrane of vesicles [137] and even water in reverse micelles [138].

As a result of energy transfer from the heated silicon substrate into the adsorbate, the observed ultrafast increase of the axial change Δc_0 is consistent with expansion of the fatty acids solely along their aliphatic chains (20–60 ps). This efficient and directional energy transfer within the fatty acid assembly is facilitated by the unique substrate heating. As discussed in chapter 4, the initial ultrafast heating induces

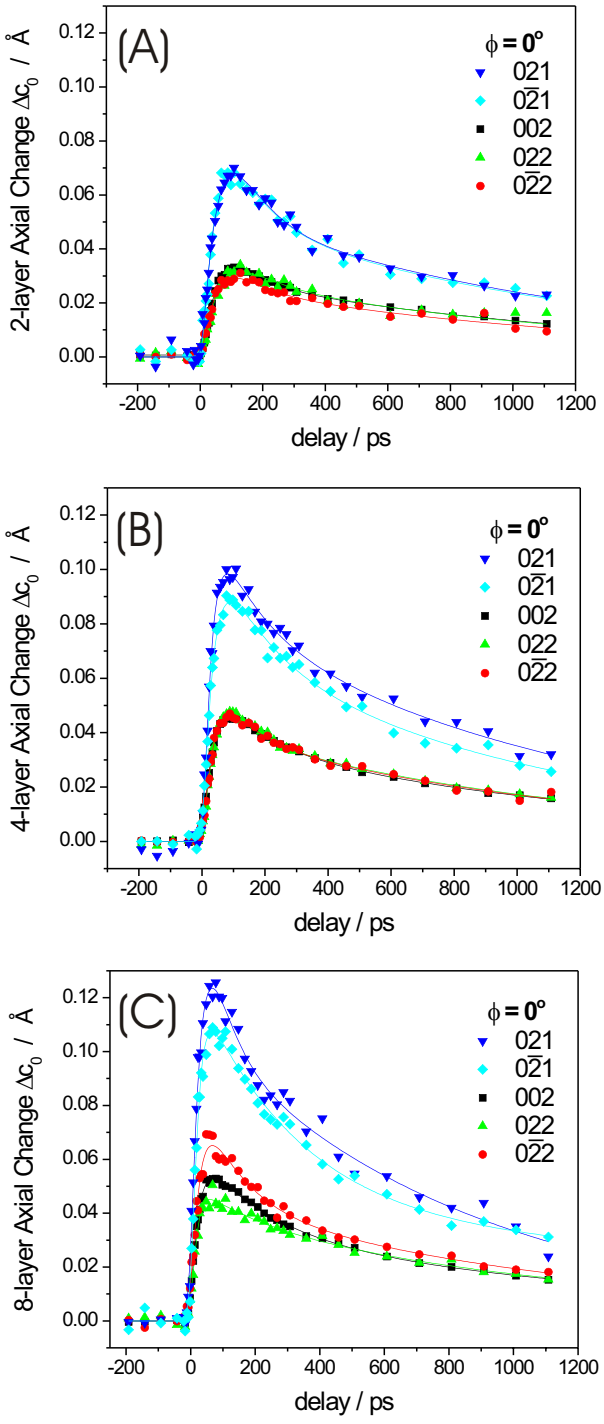

Figure 6.5: The molecular axial length change Δc_0 of the CH_2 subunit cell as a function of time showing the behavior for the different diffraction spots for (A) 2-, (B) 4- and (C) 8-layer samples. The incident azimuthal angle $\phi = 90°$. The Bragg spots are those indexed in the static diffraction patterns shown in figure 5.10, for films deposited at pH = 6.4 and $\pi = 29$ mN/m [71].

a potential-driven lattice change in the material and this results in a surface displacement which for the case discussed here acts as a directional force. It should be mentioned that the surface heating area by the laser is much larger than the absorption depth in the substrate, and this gradient of stress (temperature) facilitates the c-direction change. Moreover, the transfer within the chain is much more efficient than across the chains because of covalent bonding, as opposed to the relatively weak interactions across the chains. The elongation is followed by nonequilibrium contraction and restructuring due to energy redistribution and diffusion at longer times (60–230 ps and 1.2–1.5 ns). This behavior is indicative of two regimes of structural dynamics, that of nonequilibrium coherent motion of atoms at short time, and the evolution toward equilibrium at longer times.

The inclined chains provide an opportunity to test the nature of the expansion in directions other than perpendicular. Their inclined diffraction patterns are shown in figure 6.6 for the 8-layer sample deposited at $\pi = 29$ mN/m and pH $\simeq 7$. After the temperature jump, the smeared diffraction lines move down along the direction perpendicular to their longitudinal axis on the CCD, as shown in figure 6.6(A) for various diffraction difference images. The amplitude and time behavior of the change in the lattice spacing is comparable to that of a nontilted pattern as shown in figure 6.6(B), which is calculated from the s change for the $(hk2)$ line along the inclined direction. The dynamics of the nontilted pattern is shown for the (002) Bragg spot of the 8-layer calcium arachidate sample deposited at pH = 6.4 and $\pi = 29$ mN/m.

This observation of tilted line movement is in total agreement with the heating pulse initiating an expansion and contraction solely along the fatty acid carbon chains. The fact that the lines move along the inclined direction rather than the direction perpendicular to the shadow edge also excludes other effects which could force the Bragg spots to move in the diffraction patterns — for example charging effects or direct beam movements.

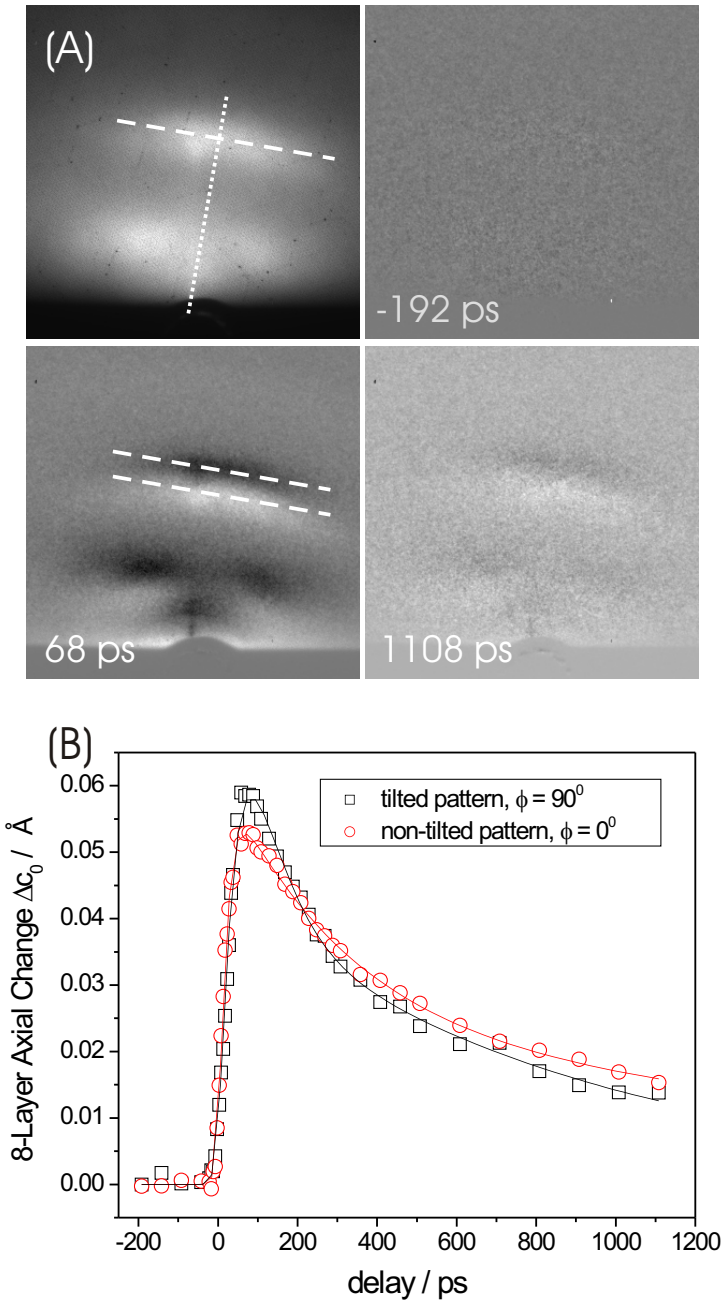

Figure 6.6: Diffraction difference patterns at $\phi = 0°$ and the axial change Δc_0 of the inclined 8-layer sample deposited at pH $\simeq$ 7 and $\pi = 29$ mN/m. (A) The static diffraction pattern before laser irradiation shows an inclination of $\sim 10°$. The diffraction difference images show the movement of the smeared lines along the direction of the aliphatic carbon chains. (B) The axial change of c_0 for the inclined fatty acids LB films at $T = 300$ K in comparison with the changes for the noninclined 8-layer sample deposited at pH = 6.4 and $\pi = 29$ mN/m at $\phi = 90°$ (see figure 5.10) [71].

6.1.2 Transient structural ordering

In figure 6.7, the relative integrated intensity changes I/I_0 of the (002) Bragg spots as a function of time for the 2-, 4- and 8-layer samples are depicted. Even though we show only transient intensity behavior of the (002) Bragg spot, the intensities of the other Bragg spots exhibit similar trends. All samples show comparable transient intensity change.

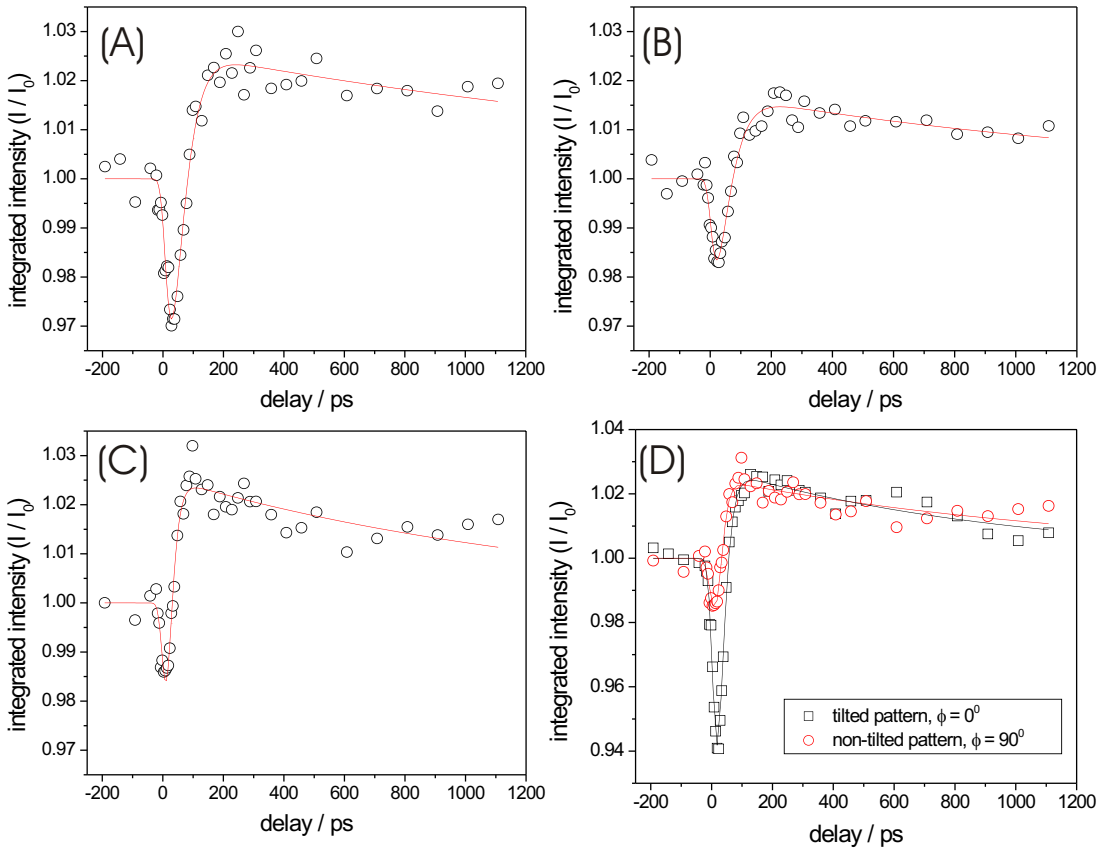

Figure 6.7: Relative intensity change I/I_0 as a function of time for (A) 2-, (B) 4- and (C) 8-layer samples, deposited at pH = 6.4 and π = 29 mN/m, at incident angle ϕ = 90°. (D) The relative intensity change I/I_0 for the inclined fatty acids LB films, deposited at pH $\simeq$ 7 and π = 29 mN/m, at incident angle ϕ = 0°, in comparison with the changes for the noninclined 8-layer sample [71].

For "conventional" heating, the intensity is expected to initially drop and subsequently recover back to the initial value, similar to the trend observed for the Bragg spot center position, Δc_0. This intensity drop follows the influence of the incoherent

motions of the atoms, which are described by the Debye-Waller factors, and structural changes due to phase transitions (see figure 5.7 and 5.8 for the static temperature behavior). For the fatty acids the transient behavior is much different from that observed at steady-state. We observe only a very short lived intensity drop on the ultrafast timescale, on the order of tens of ps. This initial drop is consistent with a disorder-induced heating, as it represents a decrease in intensity. However, after this initial decrease, the intensity recovers also fast and even gains more intensity from that of the initial value. The fact that the transient intensity is higher than the initial one indicates the formation of a transient structure with a higher degree of order. We term this behavior transient structural ordering.

Interestingly, the intensity change mirrors the line width behavior as shown, e.g., in figure 6.2(C) and (D). The line width of the Bragg spots reflects the order of the crystalline structure, and is narrower for a more ordered state. This trend is again consistent with transient structural ordering, which can be understood using the following picture, schematically depicted in figure 6.8.

Initially, the dynamics follow the expected loss of order due to rapid thermal motions similar to that observed in the early stage of the static temperature dependence; note that the lower part of figure 6.8 is similar to that shown in figure 5.9. A static temperature rise results in an expansion of the fatty acid lattice along a_0 and b_0 (see figure 5.8(B)), whereas upon laser pulse heating the energy is mainly transferred along the aliphatic chains, which results in a large increase in c_0. By overcoming some energy barrier and through alignment of the aliphatic chains and other motions (rotation, bending, etc.), and possibly through transient annealing of the film, the fatty acid molecules find an energetically more favorable structure in the film. As a result, the formerly imperfect structure transforms into a more ordered system. Because of energy dissipation on the nanosecond time scale, the film eventually restructures to its initial state. The Bragg spot center position, intensity and the line width recover toward their equilibrium values with ns recovery component, and on the ms scale (our laser repetition time) the signal is certainly back to the initial values.

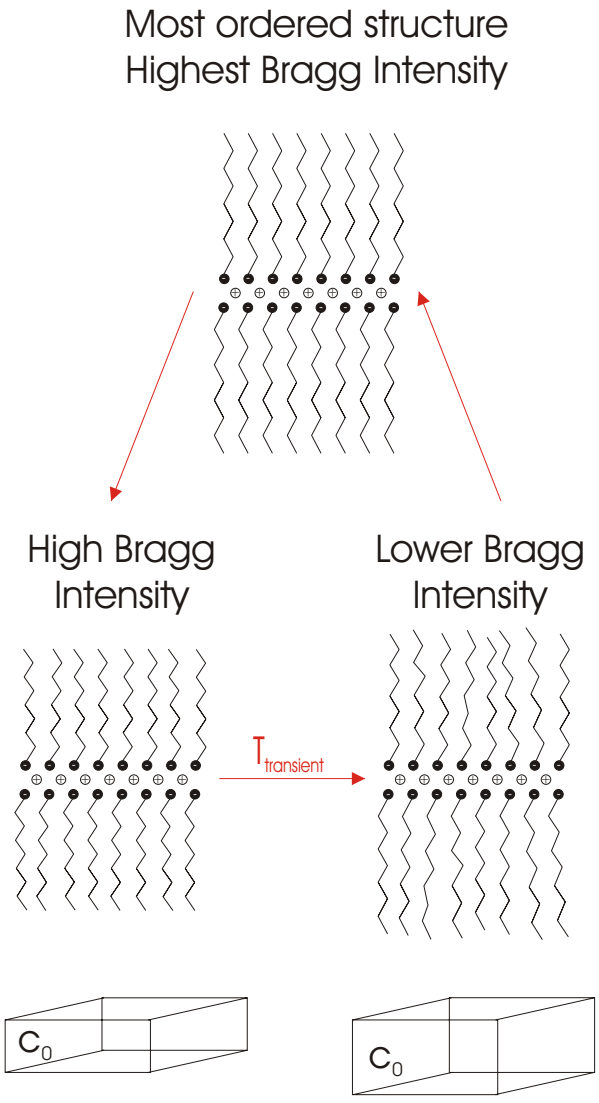

Figure 6.8: Schematic view of the transient structural ordering [71].

6.1.3 Dynamics at different static temperature

The comparison of transient and static structural changes was directly made by studying the transient behavior at different substrate temperatures. In figure 6.9 the transient axial change Δc_0 and the integrated intensity change for different static temperatures are plotted for the bilayer deposited at pH $\simeq$ 7 and $\pi = 29$ mN/m. The dynamics are shown for the (002) Bragg spot observed at $\phi = 0°$ and $T = 100$, 295 and 333 K. Indeed, the temporal behavior for the expansion and restructuring is similar for the three different temperatures, but the initial maximum amplitudes of expansion are different, increasing with increasing temperature. This trend is again consistent with the picture discussed above, namely that elevated temperatures facilitate a more pronounced expansion.

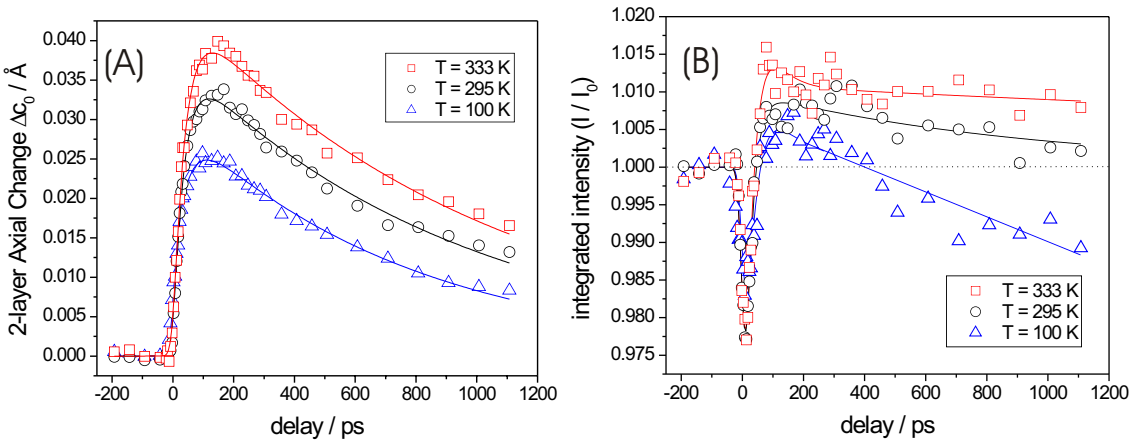

Figure 6.9: Dependence of the transient dynamics on initial substrate static temperature: $T = 100$, 295 and 333 K are shown. (A) The transient molecular axial change Δc_0 of the CH_2 subunit cell as a function of time for $\phi = 0°$. (B) The corresponding relative intensity change I/I_0 as a function of time [71].

The results shown in figure 6.9(B) further support the picture, as the intensity changes show more pronounced transient structural ordering extending over a longer time span at elevated temperatures. For $T = 295$ and 333 K the intensity recovers back to its initial value on a nanosecond timescale or larger, whereas for $T = 100$ K the transient structural ordering persists only for ~350 ps after laser pulse heating, after which the intensity drops below the initial value again, and therefore resembles

the conventional Debye-Waller behavior. This strengthens the view that expansion along c_0 and preparation of the ordered state are not two unrelated processes, but are facets of the same underlying molecular motions.

In summary, all investigated fatty acid adsorbates show expansion and restructuring along the fatty acid carbon chains. From the transient and static diffraction behavior with time and temperature, it is shown that transient structural ordering on the ultrafast timescale, initiated by laser pulse heating, is a common feature of these layered structures. Such transient structures, their anisotropy of expansion, and inhomogenity would remain unrevealed without the resolutions of UEC.

6.2 Phospholipid structural dynamics

For phospholipids, the diffraction patterns contain mainly the $(hk2)$ line, as discussed in section 5.6. Figure 6.10 displays the static diffraction patterns and the diffraction difference patterns at various delay times after the fs laser-initiated temperature jump in the underlying substrate, for DMPA monolayer and bilayer film respectively. The patterns show no features at negative times, and at positive times, mainly a change in the $(hk2)$ line position, becoming dark at the higher s value and bright at the lower s value, indicating a downward movement of the diffraction line. This translates to an increase of the -CH_2-CH_2-CH_2- distances along the aliphatic chains.

As before, we were able to fit the diffraction line with a Voigt function in the vertical s direction, providing us with accurate center position and intensity changes with time, as shown in figure 6.11(A) and (B) for the monolayer and bilayer, respectively. The error range for the width did not permit accurate values.

The dynamics of the center position change is similar for both samples, monolayer and bilayer, and are similar to the behavior observed for fatty acids. An increase in c_0 within $\sim$50 ps was observed with a recovery on the $\sim$500 ps and longer time scale. This similarity in trend is not surprising since we are probing the structural dynamics of the aliphatic chains, and in this respect DMPA resembles the fatty acid samples. It is known that for phospholipids there exist different phases ("gel" and "liquid")

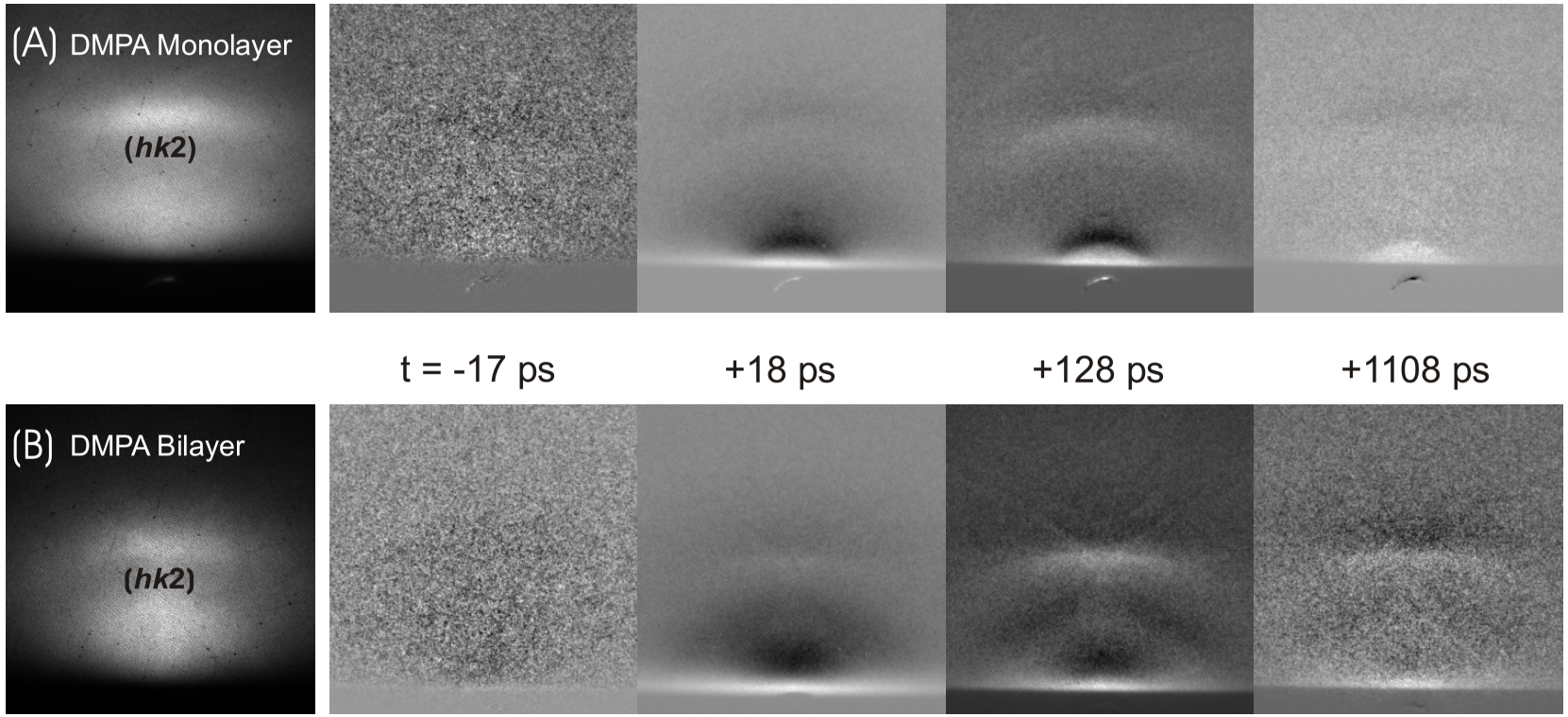

Figure 6.10: Static diffraction and diffraction difference patterns of DMPA monolayer (A) and bilayer (B). The diffraction difference patterns are shown with the time delays indicated [29].

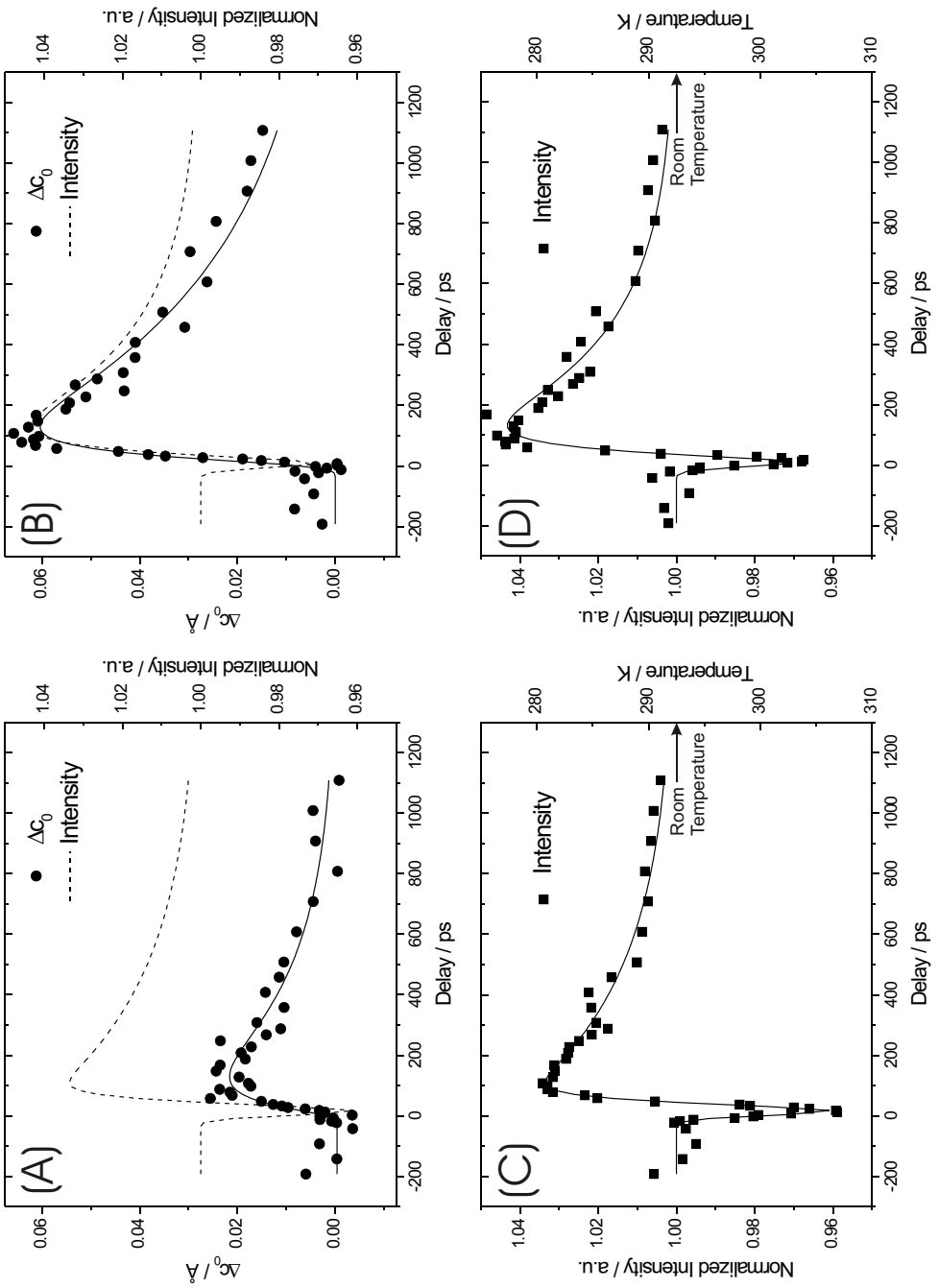

Figure 6.11: The axial change Δc_0 and the normalized integrated intensity of the $(hk2)$ diffraction line as a function of time, (A) and (C) for the monolayer and (B) and (D) for the bilayer of the phospholipid [29, 71].

and it is interesting that neutron scattering studies give a lifetime of 17 ps for the acoustic phonon excitation in the gel phase [139].

As shown in figure 6.11(A) and (B), the amplitude of the expansion for the bilayer is nearly three times that of the monolayer. A similar trend was observed for samples of 2-, 4- and 8 layers of fatty acids (see figure 6.5), but with smaller differences. This larger change of amplitude may be because the first layer exhibits different forces than the subsequent layers as it is directly bound to the silicon substrate. If the interaction forces are stronger than in the subsequent layers, we expect a tighter binding to the substrate and an increased order in the first layer, resulting in less mobility for expansion. It is interesting that for bilayers of fatty acids and phospholipids the expansion of the former is nearly half that of the latter, suggesting a bigger flexibility for expansion in phospholipids, which is again consistent with the above mentioned picture. The monolayer was studied on a hydrophilic surface, unlike the bilayer, and this is entirely in line with the proposed strong interaction with the substrate.

The intensity changes with time are also shown in figure 6.11. As in the case of the fatty acids, initially an intensity drop is recorded, consistent with the disorder being induced within 15 ps by the heating pulse. After this change the intensity increases to a value above the static one within $\sim$130 ps, before final recovery toward the initial configuration at $\sim$400 ps and longer times. The transient state of increased intensity is indicative of transient structural ordering, as discussed above for fatty acid structures. The temperature scale given in figure 6.11 is from the static intensity change as a function of equilibrium temperature (figure 5.8(A)) for a fatty acid bilayer. In the simplest model of harmonic chains, a change of 0.02 Å corresponds to a temperature increase of approximately 30 K, in the nonequilibrium regime.

In conclusion, the phospholipid monolayer and bilayer samples of DMPA show a transient behavior similar to that of fatty acids, both being adsorbates on a substrate. We observed elongation along the aliphatic chains following the ultrafast temperature jump, accompanied by transient structural ordering. The similarity is not surprising because structural changes involve the -CH_2-CH_2-CH_2- subunit cell. However, the amplitude of expansion, the influence of substrate forces, and the mobility of the

structure are found to have differences.

6.3 Structural dynamics picture

In chapter 4, it was demonstrated that ultrafast dynamics and heating of materials with a band gap are directly evident in the change with time of Bragg diffraction spot positions, their intensities and widths. The mechanism for the generation of the temperature jump is basic: the femtosecond infrared pulse excites carriers which then by electron-phonon coupling heat up the lattice and the material sustains the lattice temperature until diffusion of heat takes place on a much larger time scale. Because of the change in potential by carrier excitation and the fact that the excited region with the laser pulse is much larger than the absorption length, the gradient change is perpendicular to the surface of the material. This gradient results in a large expansion of surface atoms which is a force on the ultrashort time scale [140].

This T-jump of the material (substrate) — or the force of surface atoms — is exploited to heat up the adsorbate in a direct contact with either a hydrophobic or hydrophilic substrate; the femtosecond infrared pulse has no resonance for absorption to the adsorbate. Such studies made here for monolayers, bilayers and multilayers of fatty acids and phospholipids provide an opportunity to study structural dynamics at these interfaces on the nanometer scale, and to examine changes due to the transition from two-dimensional to three-dimensional. To achieve crystallinity, we use the methodology of Langmuir-Blodgett film, providing control over pH, thickness and pressure.

Four types of UEC measurements make possible the study of structural dynamics: the change of position with time of Bragg spots; the temporal evolution of the diffraction intensity change; the increase/decrease in diffraction width; and the change of diffraction with angle of incidence θ_i (rocking curve) and azimuthal angle ϕ for the position of the electron pulse relative to the zone axis of the substrate (see figure 5.3). As shown above, these measurements can be made with the sensitivity achieved in UEC. Prior to these measurements, we establish the static (time-averaged) structures

of the adsorbates (fatty acids and phospholipids) by determining the orientation of the chains relative to surface plane, and the -CH_2-CH_2-CH_2- chain distances which are the subunit cell dimensions a_0, b_0 and c_0.

The transient anisotropic change in c_0 of fatty acid and phopholipid layers is vastly different from that observed in the steady-state equilibrium state. At equilibrium, we observe changes in a_0, b_0 (not c_0) and the diffraction intensity only decreases to reflect thermal, incoherent motions (Debye-Waller effect) and phase transitions. On the ultrafast timescale, the expansion is along c_0, unlike the thermal case, and the amplitude of change is far larger than predicted by incoherent thermal expansion. The expansion amplitude depends on layer thickness and the nature of bonding to the substrate (hydrophilic vs. hydrophobic). The intensity and width changes are also very different from those observed by equilibrium heating, showing a transient structural ordering in tens of ps.

Following the initial ultrafast heating, the structure first expands (atomic displacements) along the c-direction (compare figures 5.9 and 6.8). These motions with the acquired energy in the layers lead into transient structural ordering through "annealing" and/or chain motions, as evident from increased diffraction intensity and narrowing of diffraction width beyond the initial values. On the nanosecond and longer time scale, the structure reaches quasi-equilibrium or equilibrium (incoherent movement of atoms) and by dissipation of heat (diffusion) the structure acquires the original configuration, certainly on the millisecond time scale between pulses. This behavior is in contrast with that observed at steady state.

The net change in displacement is determined by the impulsive force ("temperature") of the substrate (including coupling), and the maximum value of the extension depends on elasticity and heat capacity. If heating occurs for an equilibrated system, the change in the value of c_0 with temperature Δc_0 (by anharmonicity) should be independent of the number of -CH_2-CH_2-CH_2- subunits in the chain, and $\Delta c_0/c_0$ becomes simply α (the thermal expansion coefficient), which is typically very small $\Delta c_0/c_0 \simeq 10^{-5}T^{-1}$) [141]; for a 10-degree rise, this expansion would be on the order of 10^{-4} Å, while the observed transient change is as large as 0.01 Å. For nonequilibrium

dynamics in the chains, this large amplitude is understood even for harmonic chains.

The impulsive force at short times transmits a large change in the value of Δc_0 as the disturbance (wave-type) accumulates to give the net effect that is dependent on the number of C atoms [142]. In other words, as the disturbance passes through the different bonds, the diffraction amplitude builds up and exhibits a delay, ultimately giving a rise and large total amplitude for the change. This picture also explains the dependence on the total length of the chains, the increase in initial maximum amplitude as the temperature of the substrate increases, and the effect of substrate strong (hydrophilic) vs. weak (hydrophobic) binding. Quantification of the total change must take into account the nature of the substrate force and variation in the density of the LB films upon going from single to multiple layers. It is known that "defects" or "holes" can be formed when multiple layers are deposited [88], and that disorder is expected as the influence of the substrate subsides.

The fact that the initial change in intensity (and elongation) occurs on the 10 ps time scale and that the distance traveled is approximately 20 Å (for a monolayer) the speed of propagation should be sub-kilometers per second, which is close to the propagation of sound waves. Because the substrate is heated through optical and acoustic phonons (see chapter 4), the rise is convoluted with the process of phonon generation which is on the time scale of 10 ps; we note that the resolution imposed by the geometry of electron and light propagation on the surface is $\sim$1–2 ps. Accordingly, the speed could be of higher value reaching the actual speed of sound in the layers. Future experiments will further resolve this region to elucidate the maximum extension possible and the expected coherent features. The coherent coupling among bonds in the underdamped regime of harmonic motions is vastly different from the diffusive behavior in the overdamped regime.

The force and vibrational frequencies of -CH_2-CH_2-CH_2- motions in the diffusive (overdamped) regime have to be unrealistically large [142]. In the underdamped regime, although the force is significant to cause the large change in Δc_0, and coherent propagation is within the chain, the change in the value of Δc_0 relative to that of c_0 is relatively small to preserve the robustness of the Bragg spots throughout the

temporal change. It is important to point out that for large complex systems the diffraction has features of both "crystalline" and "diffusive" scattering. The latter gives structural information on the collective motions, which can be examined through cross-terms of the Debye-Waller factors [143]. In this regard, the ring(s) apparent at $s \simeq 0.3$ Å^{-1} in the diffraction difference patterns in figure 6.10 should be analyzed for such correlations in the phospholipid, and in future work we shall consider this analysis.

Besides the analytical theoretical work discussed above, in collaboration with Professor T. Shoji and colleagues in Japan, we have studied MD simulations of a prototype system. The model used is that of a silicon substrate with the adsorbates made of $C_{20}H_{42}$ chains, covering a total combined length of 95 Å. The potentials for the chains, substrate and the interaction at the interface were from *ab initio* calculations. The time step was 0.5 fs and the total number of steps was 200,000. The heat pulse was modeled based on the kinetic energy of the substrate atoms. The radial distribution function and the actual vibration motions of the atoms were obtained at different times, and we considered both the self-assembly and the confined geometry of the chains. These calculations provided the structural cell dimensions observed experimentally, and elucidated the coherent motion in the chain bonds and their time scales. Preliminary results show the increase in -CH_2-CH_2-CH_2- distance near the silicon surface by 0.08 Å in about 5 ps.